

Electronic Supplementary Material (ESI) for New Journal of Chemistry
This journal is © The Royal Society of Chemistry 2022

Supporting Information

Ultra-sensitive hydrogen peroxide electrochemical sensor based on dual-phase perovskite oxide tubular nanofiber

Xin Qu, Siyu Zhao, Peixiang Gao, Xin Qian, Shuanglong Lu, Fang Duan, Han Zhu,

Mingliang Du*

Key Laboratory of Synthetic and Biological Colloids, Ministry of Education, School of Chemical and Material Engineering, Jiangnan University, Wuxi 214122, P. R. China.

Email: du@jiangnan.edu.cn

Fig. S1 (a) The EDS spectra and (b) Comparison of ICP-OES and EDS results of dual-phase LaSrNiO NFs.

Fig. S2 (a) FT-IR spectra of LaNiO NFs and LaSrNiO NFs.

Fig. S3 CV curves of LaSrNiO NFs at different temperatures with or without 2.5 mM H₂O₂: (a) 500 °C, (b) 600 °C, (c) 700 °C, (d) 800 °C, (e) 900 °C, (f) 1000 °C.

Fig. S4 (a) CVs of the LaSrNiO/GCE-700 obtained in 0.1 M NaOH with 0.5 mM H₂O₂, scan rate:100 mV/s. (b) CV curves of the LaSrNiO/GCE-700 obtained in 0.1 M PBS with 0.5 mM H₂O₂, scan rate:100 mV/s.

Fig. S5 (a) The CVs of (a)Bare GCE, (b) LaNiO/GCE-700, and (c) LaSrNiO/GCE-700 obtained in 0.1 M NaOH with and without 1 mM H₂O₂, scan rate:100 mV/s.

Fig. S6 CV curves of (a) LaNiO/GCE-700 and (c) LaSrNiO/GCE-700 obtained at different scan rates (50 ~ 100 mV/s). The corresponding linear relationship between the scan rate and the current density of (b) LaNiO/GCE-700 and (d) LaSrNiO/GCE-700.

Fig. S7 (a) The linear relationship of CV reduction peak potential versus lnν for laSrNiO/GCE-700 at different scan rates.

Fig. S8 Amperometric response of (a) LaNiO/GCE-700 and (b) LaSrNiO/GCE-700 at 0.1 M NaOH with 100 μM H₂O₂.

Table S1 Performance comparison of different hydrogen peroxide detection techniques.

Table S2 Comparison of the performance of different perovskite materials for hydrogen peroxide sensing.

1. Materials and instruments

Lanthanum nitrate hexahydrate ($\text{La}(\text{NO}_3)_3 \cdot 6\text{H}_2\text{O}$, AR, 99%), strontium nitrate ($\text{Sr}(\text{NO}_3)_2$, AR, 99%), nickel nitrate ($\text{Ni}(\text{NO}_3)_2 \cdot 6\text{H}_2\text{O}$, AR, 99%) and polyvinyl pyrrolidone (PVP, $M_w \approx 1.3 \times 10^6$) were commercially available from Shanghai Macklin Biochemical Technology Co., Ltd. Ethanol absolute ($\text{CH}_3\text{CH}_2\text{OH}$, 99.7%), N, N-Dimethylformamide (DMF, AR, 99.5%), KH_2PO_4 , K_2HPO_4 , $\text{K}_2\text{S}_2\text{O}_8$, and Nafion solution were purchased from Sinopharm Chemical Reagent Co., Ltd. H_2O_2 , NaOH, ascorbic acid (AA), bisphenol A (BPA), glucose, KI and formaldehyde (HCHO) were all bought from Sinopharm Chemical Reagent. 2, 2'-azino-bis (3-ethylbenzothiazoline-6-sulfonic acid) free radicals (ABTS) were bought from Merck KGaA (ABTS reacts with $\text{K}_2\text{S}_2\text{O}_8$ to form ABTS^{•+} free radicals). 1,1-diphenyl-2-picryl-hydrazyl radical (DPPH[•]) was bought from Med Chem Express. All solutions were prepared using distilled water and all chemicals were used without further treatment.

The morphology and structure of the products were investigated by the scanning electron microscopy (SEM, HITACHI S-4800, Japan), the transmission electron microscopy (TEM, JSM-2100, JEOL, Japan), the scanning transmission electron microscopy (STEM, Tecnai G2 F30S-Twin, Philips-FEI) at an acceleration voltage of 300 kV. The contents of different metal elements were analyzed by energy dispersive spectroscopy (EDS, HITACHI S-4800, Japan) and inductively coupled plasma optical emission spectroscopy (ICP-OES, Aglient 5110). The crystal phases were furtherly analyzed by X-ray diffraction (XRD) with Cu K α radiation ($K = 1.5418 \text{ \AA}$) at a scanning rate of 0.02° in the 2θ range of 10 ~ 80°. The Fourier transform infrared (FT-IR, Nicolet 6700, America) spectra investigate the changes in the functional groups of structural features. The elemental composition of the products was investigated by X-ray photoelectron spectra (XPS) on a Kratos Axis Ultra DLD at an acceleration voltage of 15 kV. Electron paramagnetic resonance (EPR, Bruker EMX Plus) was used to investigate the intensity of oxygen vacancy under the air atmosphere.

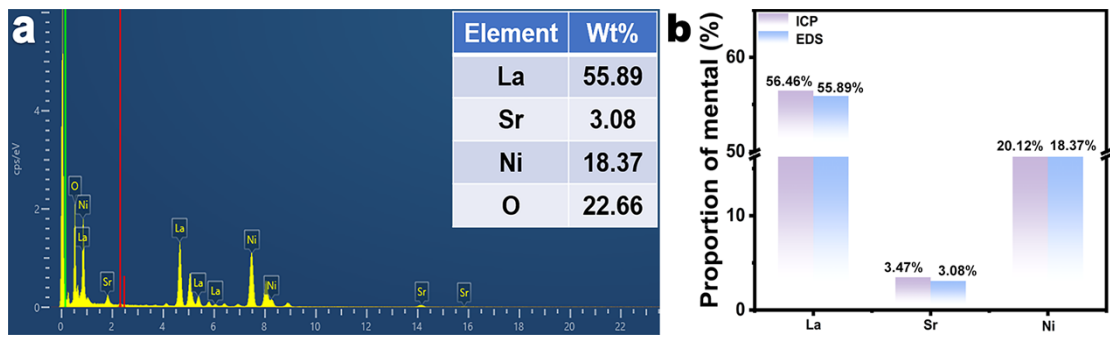


Fig. S1 (a) The EDS spectra and (b) Comparison of ICP-OES and EDS results of dual-phase LaSrNiO NFs.

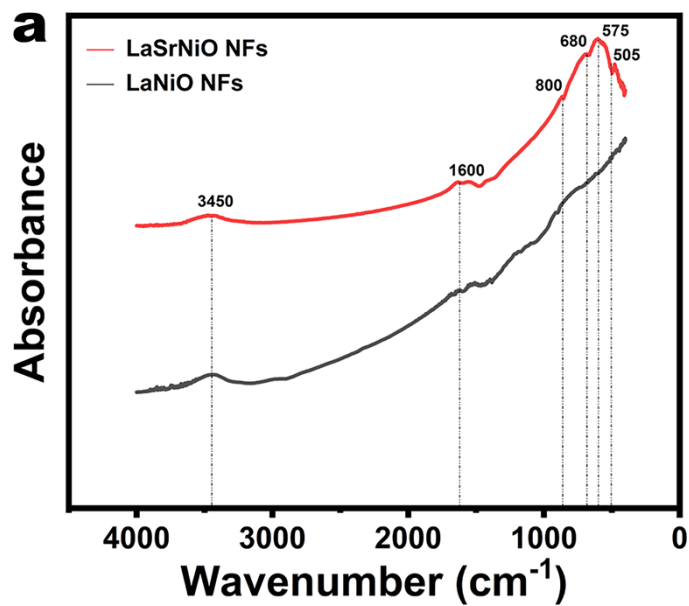


Fig. S2 (a) FT-IR spectra of LaNiO NFs and LaSrNiO NFs.

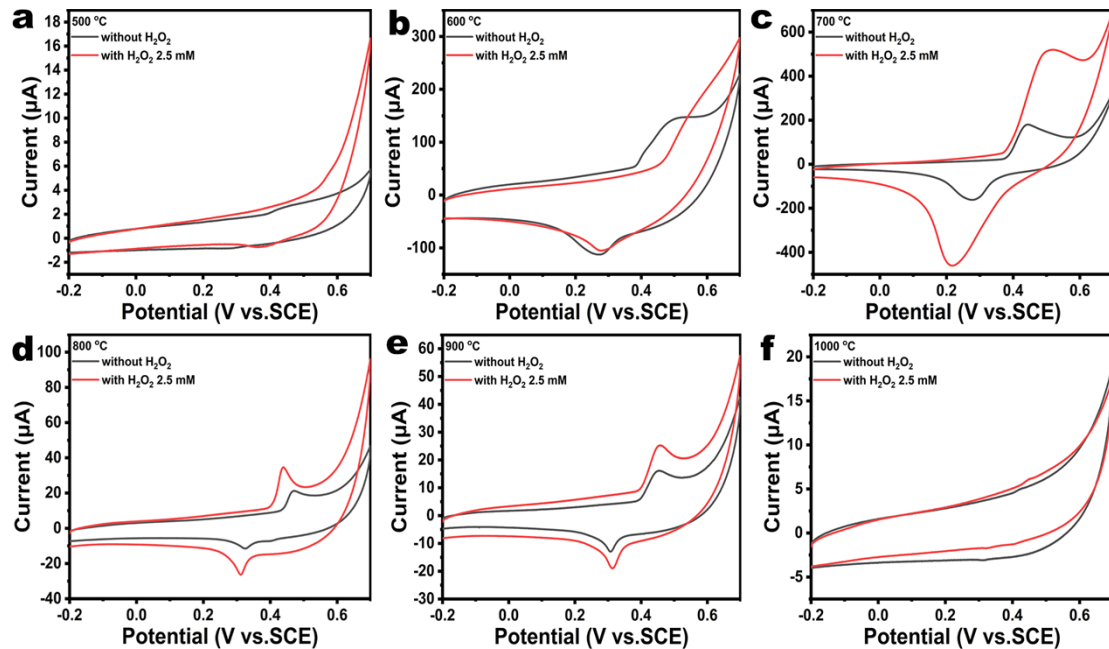


Fig. S3 CV curves of LaSrNiO NFs at different temperatures with or without 2.5 mM H_2O_2 : (a) 500 $^{\circ}\text{C}$, (b) 600 $^{\circ}\text{C}$, (c) 700 $^{\circ}\text{C}$, (d) 800 $^{\circ}\text{C}$, (e) 900 $^{\circ}\text{C}$, (f) 1000 $^{\circ}\text{C}$.

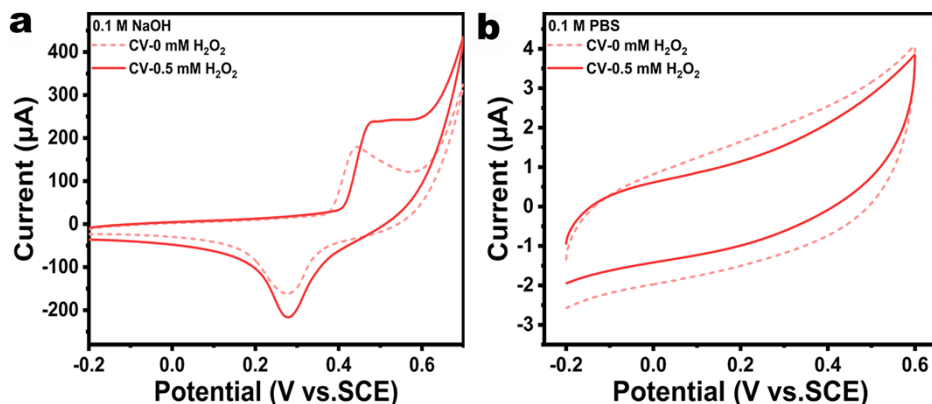


Fig. S4 (a) CVs of the LaSrNiO/GCE-700 obtained in 0.1 M NaOH with 0.5 mM H_2O_2 , scan rate: 100 mV/s. (b) CV curves of the LaSrNiO/GCE-700 obtained in 0.1 M PBS with 0.5 mM H_2O_2 , scan rate: 100 mV/s.

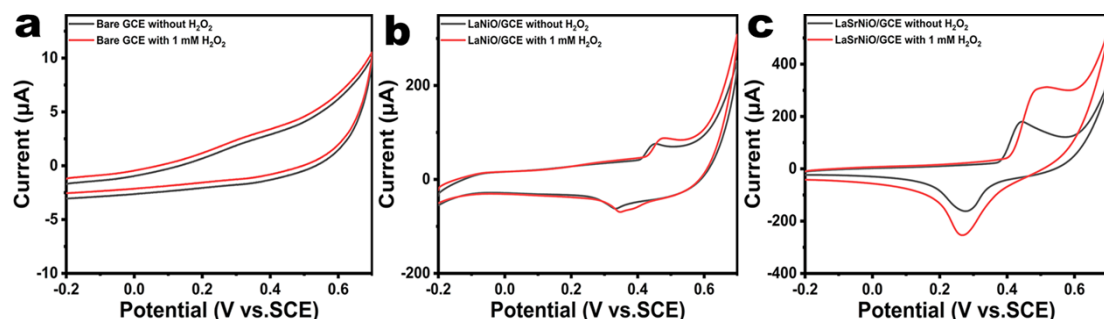


Fig. S5 (a) The CVs of (a) Bare GCE, (b) LaNiO/GCE-700, and (c) LaSrNiO/GCE-700 obtained in 0.1 M NaOH with and without 1 mM H_2O_2 , scan rate: 100 mV/s.

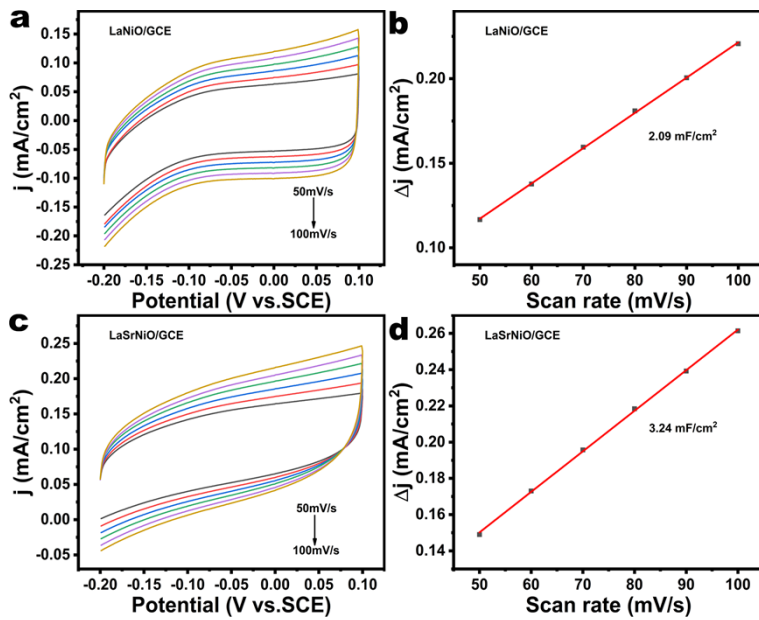


Fig. S6 CV curves of (a) LaNiO/GCE-700 and (c) LaSrNiO/GCE-700 obtained at different scan rates (50 ~ 100 mV/s). The corresponding linear relationship between the scan rate and the current density of (b) LaNiO/GCE-700 and (d) LaSrNiO/GCE-700.

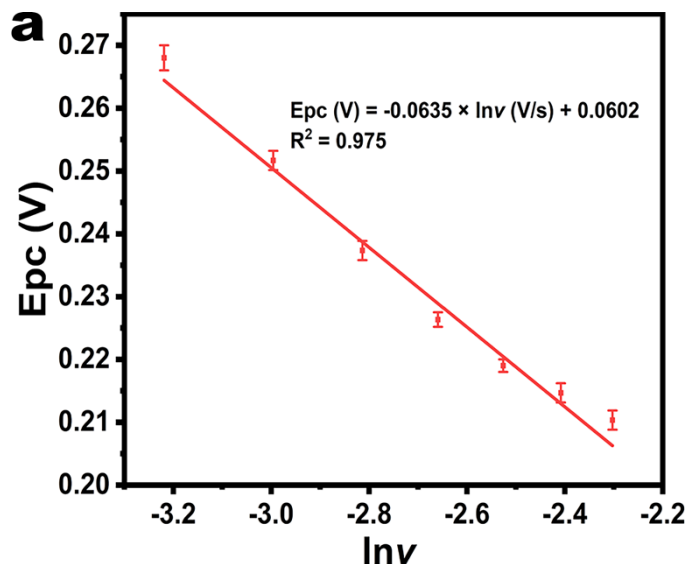


Fig. S7 (a) The linear relationship of CV reduction peak potential versus Inv for LaSrNiO/GCE-700 at different scan rates.

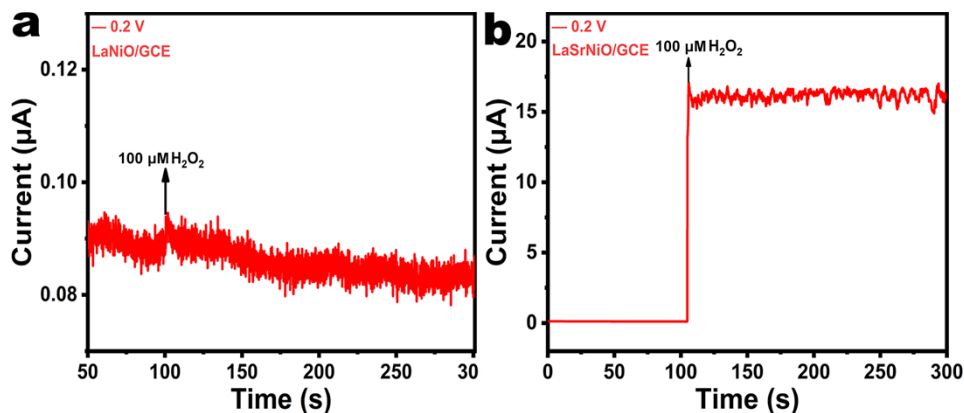


Fig. S8 Amperometric response of (a) LaNiO/GCE-700 and (b) LaSrNiO/GCE-700 at 0.1 M NaOH with 100 μM H₂O₂.

Table S1 Performance comparison of different hydrogen peroxide detection techniques.

Methods	LOD (μM)	Sensitivity ($\mu\text{A} \cdot \text{mM}^{-1} \cdot \text{cm}^2$)	Linear range (μM)	reference
A novel quinoxalinamine based fluorescent probe	0.046	--	--	1
A near-infrared fluorescent probe	0.065	-	0~7	2
Near-infrared fluorescence probe	0.14	-	-	3
Boronate-Based fluorescence	-	--	10	4
Fluorescent Fe ₃ O ₄ Quantum Dots	0.0038			5
Colorimetric H ₂ O ₂ Detection	10	0.1-1000		6
Electrochemical	0.018	1667.9	10-7000	This work

Table S2 Comparison of the performance of different perovskite materials for hydrogen peroxide sensing.

Catalysis	Potenti al (V)	LOD (μM)	Sensitivity ($\mu\text{A} \cdot \text{mM}^{-1} \cdot \text{cm}^2$)	Linear range (μM)	reference
Co _{0.4} Fe _{0.6} LaO ₃	0.55 V	0.002	2376.7	0.01-800	7
La _{0.7} Sr _{0.3} Mn _{0.75} Co _{0.25} O ₃	-	0.17	1371.5	0.5-1000	8
Sr _{0.85} Ce _{0.15} FeO ₃	0.4 V	10	60	0-500	9
LaNi _{0.6} Co _{0.4} O ₃	0.55 V	0.001	1218.84	0.01-100	10
La _{0.1} Sr _{0.9} NiO ₃ NFs	0.2 V	0.018	1667.9	10-7000	This work

rGO: Reduced Graphene Oxide

CPE: Carbon Paste Electrode

References

1. M. Yang, Y. S. Wang, W, Y. Huang, and M. Ji, *Spectrochim. Acta A Mol. Biomol.*, 2022, **267**, 120528.
2. X. Huang, Z. P. Li, Z. X. Liu, C. C. Zeng, and L. M. Hu, *Dyes Pigm*, 2019, **165**, 518–523.
3. J. H. Zhang, L. Shi, Z. Li, D. Y. Li, X. W. Tian, and C. X. Zhang, *Analyst*, 2019, **144**, 3643.
4. E. W. Miller, O. Tulyathan, E. Y. Isacoff, and C. J. Chang, *Nat. Chem. Biol.*, 2007, **3**, 263–267.
5. S. R. Ahmed, J. Cirone, and A. C. Chen, *ACS Appl. Nano Mater.*, 2019, **2 (4)**, 2076–2085.
6. Z. K. Zhang, Q. Q. Liu, Y. M. Liu, R. Qi, L. L. Zhou, Z. J. Li, J. Yun, R. J. Liu, and Y. Q. Hu, *Nano*, 2020, **15**, 2050009.
7. Z. Zhang, S.Q. Gu & Y.P. Ding, F.F. Zhang and J.D. Jin, *Microchim Acta*, 2013, **180**, 1043–1049.
8. D. Xu, L. Li, Y.P. Ding, and S.Q. Cui, *Anal. Methods*, 2015, **7**, 6083–6088.
9. F. Deganello, L.F. Liotta, S.G. Leonardi and G. Neri, *Electrochim. Acta*, 2016, **190**, 939–947.
10. Z. Zhang, S.Q. Gu, Y.P. Ding, and J.D. Jin, *Anal. Chim. Acta*, 2012, **745**, 112–117.